frontiers | Frontiers in Materials

TYPE Original Research
PUBLISHED 26 October 2023
DOI 10.3389/fmats.2023.1220421

OPEN ACCESS

EDITED BY
Ilkwon Oh,
Korea Advanced Institute of Science and Technology (KAIST), Republic of Korea

REVIEWED BY
Seung Hee Jeong,
Harvard University, United States
Kwang Kim,
University of Nevada, Las Vegas, United States

*CORRESPONDENCE
Yauheni Sarokin,
yauheni@ut.ee
Indrek Must,
indrek.must@ut.ee

RECEIVED 11 May 2023
ACCEPTED 13 October 2023
PUBLISHED 26 October 2023

CITATION
Sarokin Y, Aabloo A and Must I (2023), Charge-controlled swelling gradients at 200-µm resolution in an open-porous polymeric structure for compliance modulation.
Front. Mater. 10:1220421.
doi: 10.3389/fmats.2023.1220421

Charge-controlled swelling gradients at 200-µm resolution in an open-porous polymeric structure for compliance modulation

Yauheni Sarokin*, Alvo Aabloo and Indrek Must*

Institute of Technology, University of Tartu, Tartu, Estonia

Plants combine active and passive liquid-mediated mechanisms across broad spatial and temporal scales, inspiring technological developments, in particular involving variable stiffness. Swelling is of particular interest due to the abundance of plant models and applicable (bio)materials, yet existing control by environmental humidity sorption limits its applications. This work combined swellable polymeric structures with electroactive control: we considered an open-porous polymeric laminate that hosted an electrokinetic medium also co-acting as a swelling agent for the same polymer. A constant volume of liquid (an electrolytic solution) was electrokinetically pumped between the symmetrical laminate's interior and surface layers: as the second moment of inertia increases from the centre to the surface, the pumping of liquid towards the surface decreases the laminate's bending stiffness, and *vice versa*. Ion electrosorption on high-specific-surface-area carbon electrodes, deposited in three layers in the laminate by simple additive spraying, facilitated the ion current necessary for the electrokinetic pumping. Flexural rigidity of the 400 µm thick laminate varied by 7% in response to 2-V input, evidencing swelling gradients forming at half-laminate (i.e., 200-µm) resolution. Charge-driven local rearrangement of liquid allows for broader adoption of bioinspired (and biological) porous architectures, where the channels are defined collectively, not individually as in, e.g., soft lithography. Sub-mm resolution and low-voltage control of liquid offer a high level of integration at minimal assembly, positioning active swelling as a promising solution for wearable and bioinspired soft robotic applications.

KEYWORDS

variable stiffness, swelling, electrosorption, electrokinetic pumping, open-porous structures, capacitive laminates, amorphous carbon

1 Introduction

Increasing achievable (approaching organism-like) task complexity by delegating interaction handling on the mechanical system of the robot's body (Mengaldo et al., 2022) is among the ongoing grand challenges in robotics. The development of physical intelligence demands not only new materials but also appropriate architecture. As one example, nature suggests a solution for an apparently contradictory demand of high load capacity and low elastic modulus–a compliant grasp to a delicate object can be established

using a soft (low-modulus) gripper and maintained (i.e., effectively 'anchoring') by rendering the same gripper more rigid (i.e., by increasing its modulus) (Fiorello et al., 2020). This strategy results in a compliant grip by minimising interfacial stress concentrations: the gripper's boundary 'self-aligns' (i.e., physically conforms) to the local loading conditions (in contact with an object) at the material level, with or without the involvement of centralised control. Therefore, technology for distributed stiffness variation at high spatial resolution in a conformable sheet form factor is in demand for enabling distributed compliance-matching scenarios. Most available actuators concurrently change their structure's stiffness to a certain degree, expressed at individual actuator level (e.g., a stepper motor stall torque increases upon activation) or by bioinspired antagonistic (Althoefer, 2018) arrangement of several actuators. Promising assembly-defined variable-stiffness solutions such as jamming (Jiang et al., 2014; Li et al., 2017; Wang et al., 2019), coupled tendons (Shiva et al., 2016; Hao L et al., 2018) and twisted rubber artificial muscles (Helps et al., 2020) do promise compliance, yet material-level compliance modulation (i.e., involving a direct change in mechanical properties of materials) (Loeve et al., 2010; Hao Y et al., 2018; Wang et al., 2018) promises an increased degree of freedom. The challenge hereby tackled is suggesting a variable-stiffness technology, the range of stiffness, and overall integration capability that satisfies the requirements for operation in contact with delicate environments such as the human body. As thermal control using phase and glass transition of materials appears to provide the best variable-stiffness metrics (stiffness variation in multiple orders of magnitude) and is easy to deploy (Loeve et al., 2010; Hao L et al., 2018; Wang et al., 2018), the physiological limits strictly limit the applicable temperature range, strongly favouring non-thermal methods. New robotic solutions with controllable stiffness at a high spatial resolution and safe in-body contact are in great demand (Manti et al., 2016; Blanc et al., 2017; Althoefer, 2018).

This work suggests a material-level variable-stiffness solution based on the internal rearrangement of an electrohydrodynamic (EHD) medium in a soft laminate. As interactions between liquids and porous polymeric matrices can readily express strain and modulus variation (Saunier et al., 2004; Metze et al., 2023), our aim is to actively rearrange a liquid within a porous structure to develop swelling gradients. Reversible interactions between PVDF polymer and ionic liquid swelling agent (Saunier et al., 2004; Shimizu et al., 2011) are known to be of suitable range to allow for the use of ionic liquids also as EHD medium. Consequently, the system performs as a variable-stiffness actuator (can be optimized for one or another), yet the form of a thin laminate enables massively distributed settings for active compliance matching beyond the reach of, e.g., tendons. The liquid rearrangement in an open-porosity matrix also implies that channels for the accommodation and transport of liquid are not defined individually, as is in the case of soft lithography (Kim et al., 2008; Qin et al., 2010). On the contrary, the liquid channels incorporated in a polymer network can be treated collectively, like natural vascular systems that may incorporate a vast capillary network. As a compromise, the open-channel networks (either a capillary network of biological tissues or a polymer matrix in natural systems) subject to liquid perfusion can be limited in spatial resolution as the liquid is subject to spontaneous rearrangement via capillary action. However, this work demonstrates active swelling at sub-mm resolution, comparable to many biological systems (e.g., skin) and well-matched to distributed (wearable) applications.

The actively driven swelling system is divided into two sequential and interdependent apparatuses: (a) providing liquid mobility (i.e., the pump): and (b) responding to the mobile liquid by swelling. This separation creates opportunities for strategic lateral separation of corresponding components or, *vice versa*, combining both functionalities into the very same component, exemplifying the highly convoluted functionality of organisms (and bioinspired soft robotics). In either strategy, the components can be deposited at the material level, with minimal assembly required, strongly encouraging the development of miniature and distributed solutions (within the resolution limit discussed above). This work opts for (and demonstrates) the highest level of integration, combining liquid-responsive components (the polymeric network) into the pumping apparatus. We chose the electrosorption of ions, with a disparity of cation and anion mobility, on high-surface-area carbon electrodes as the pumping apparatus for its high reversibility and simple constitution of the working fluid (an organic salt dissolved in a solvent). The particles of carbon are held in place by a polymeric matrix. Consequently, the swellable polymer effectively fills up the interparticle spaces in the carbon electrode, yielding the highest volume efficiency. Finally, the electrohydrodynamic medium partially fills up the space within the porous carbon as well as the porous polymer, also acting as an ion reservoir for the pumping apparatus. The ions (with mobility disparity between cations and anions) in a porous polymer matrix can be seen as miniature 'pistons' that, in addition to their displacement, may also push in front (forming a small hydraulic pressure, strongly dependent on ion-pore size match) or carry solvent molecules in their hydration sheath. Finally, the liquid influx or outflux causes swelling and deswelling of the negatively and positively charged polymer composite. The swelling effect in two-electrode ionic capacitive laminates (ICLs) has been suggested for actuation, as shown in Figures 1A–C and Supplementary Video S1, such as non-muscular (swelling as a more plant-inspired movement mechanism than muscles) biomimetic actuators (Uduste et al., 2020). Upon visual observation, it was noted that the surface of the negatively polarised electrode became wetted by an excess of liquid, giving it a shiny appearance, indicating an excess of transferred EHD medium beyond the composite electrode's pore capacity (as illustrated in Figures 1B,C). To enhance visualisation, the operating voltage was slightly increased above the nominal level to 3 V. A small amount of pressure is generated to displace liquid; however, the observed excess of liquid suggests an open porous structure of the composite electrode, implying no pressure accumulation upon liquid pumping. The influx of EHD medium also indicates increased swelling and concurrently decreased elastic modulus due to polymer affinity for the electrolytic solution (Saunier et al., 2004). While harnessing this elastic stiffness modulation change is promising for distributed configurations, it has not yet received much research attention. Although stiffness variation has likely occurred also in proof-of-concept two-electrode ICL actuators (Uduste et al., 2020), the cross-plane displacement of the EHD medium results in an increase of elastic modulus in one electrode and a decrease in the opposite, effectively cancelling each other out. The thickness

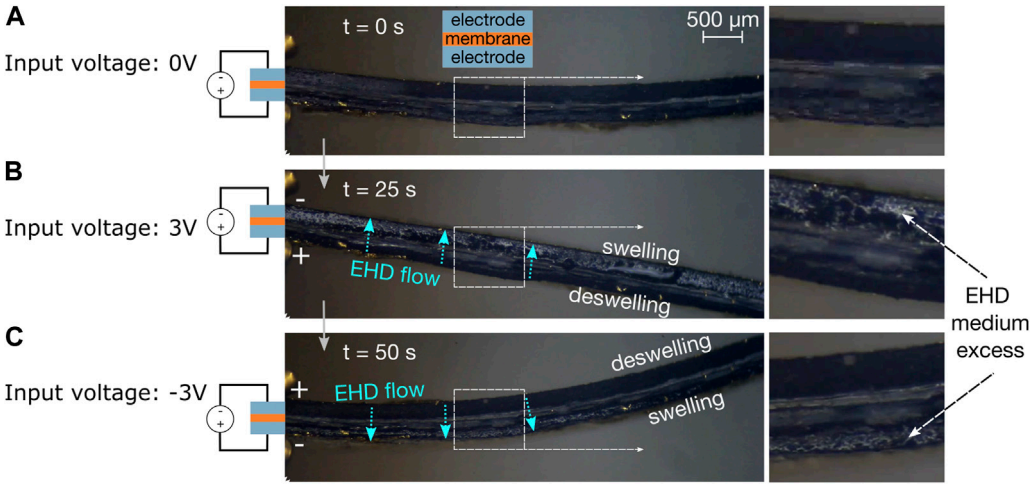

FIGURE 1
Evidence of electrohydrodynamic (EHD) medium transfer between electrodes in two-electrode laminate, causing non-uniform swelling and actuation, visually observed in the cross-section view (zoom-ins are provided at right). **(A)** Uncharged laminate, corresponding to uniform (gradient-free) EHD medium distribution; both electrodes appear visually similar. **(B)** Upon application of potential across the two electrodes, EHD medium was displaced towards the negatively polarized electrode. After saturating the pore volume, the excess of transferred EHD medium emerged at the laminate surface adjacent to the negatively polarised electrode, evidenced by the shiny area. **(C)** At reverse applied potential, the traces of EHD medium disappeared from the surface of the (now positively polarised) electrode and emerged at the opposite (now negatively polarised) electrode, evidencing transport and rearrangement of a constant volume of EHD medium within the laminate. Cyan arrows indicate the direction of EHD medium displacement.

variation of the laminate is expected to be negligibly small. This is confirmed by previous digital image correlation (DIC) investigation on bending actuators using similar composite electrodes with PVdF(HFP) binder and electrohydrodynamic medium (Punning et al., 2016), revealing 0%–0.5% variation in laminate thickness whereas the maximum local strains were substantially higher (~1%) and comparable to actuation experiment in Figure 1 (maximum strain amplitude 1.0%). We designed a three-electrode mirror-symmetric laminate that operates by displacing liquid between the internal electrode and two external electrodes (electrically connected). Upon liquid influx into the external composite electrodes, the polymeric matrix, also acting as its binder, swells in an electrolytic solution and decreases its elastic modulus. The neutral plane is not expected to vary upon pumping due to symmetric construction and activation. As the second moment of inertia of a layer is proportional to the square of the distance from the neutral plane (Goodno and Gere, 2020), the external composite electrodes, due to the largest distance from the neutral plane, are expected to give the primary contribution to laminate's bending stiffness. To the contrary, the swelling of the internal composite electrode, although comparable by magnitude and opposite in polarity, is expected to give negligible contribution to bending stiffness due to the closeness to the neutral plane (but can slightly contribute via increasing the I component of the external layers upon swelling). Elastic modulus variations in external layers are thus amplified due to the larger distance from the neutral plane. A schematic illustration of individual contributions of elastic modulus and second moment of inertia changes upon electrolytic solution displacement is depicted in Figures 2B–D. During the charging process, a change in the overall thickness of the laminate is not anticipated, as any variation in thickness within each layer of the laminate is counterbalanced by other layers due to the preservation of volume upon electrohydrodynamic medium displacement. The elastic modulus E and second moment of inertia I change at the centre electrode, regardless of its magnitude, only affects the bending stiffness by a small margin. As the centre electrode is swelling while outer electrodes are deswelling, we expect a negligible change in the laminate thickness; yet, the second moment of inertia of the external electrodes may decrease slightly due to a decrease in w (Figure 2A). As a result, external electrodes are considered to have the highest impact on the overall bending stiffness variation since the distance from the neutral plane (at the centre of the beam) is the largest. Consequently, the mirror-symmetric operation of a three-electrode laminate amplifies the polarity-dependent bending stiffness response (and disallows bending actuation to isolate the bending stiffness variation). As it is challenging to assess the individual swelling ratio (also expressed by thickness and elastic modulus variation) of each layer experimentally, this work measures the bending stiffness changes of the whole laminate, dominated by swelling of the outmost layers (i.e., the external electrodes). Figure 1D illustrates the amplified contribution of external electrodes on bending stiffness increase. The system stands out by minimum complexity and simple charge-driven low-voltage control, promising wearable applications.

2 Materials and methods

2.1 Fabrication of three-electrode ICL

Membrane solution was prepared by mixing 2 g of poly(vinylidene fluoride-co-hexafluoropropylene) (PVDF-HFP, Sigma Aldrich, M_w = 400,000), 2 g of 1-ethyl-3-methylimidazolium trifluoromethanesulfonate ([EMIM][OTf], 99.5%, Solvionic), 4 mL propylene carbonate (PC, 99%, Sigma

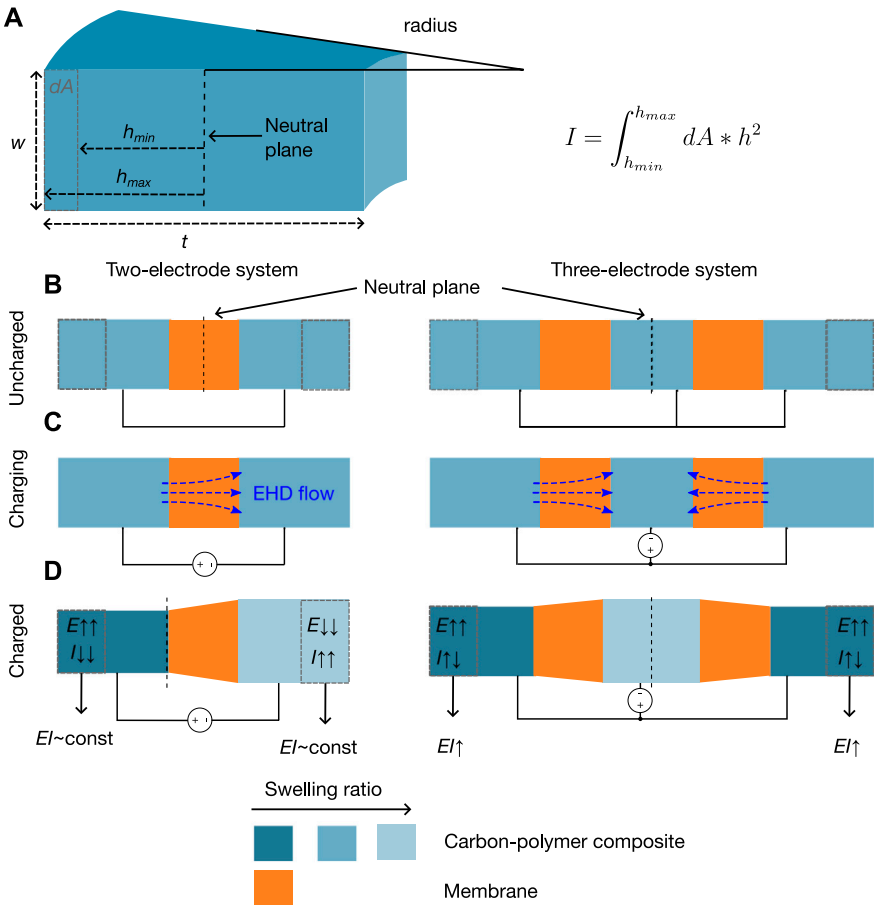

FIGURE 2
The concept of electrohydrodynamic (EHD) medium transfer in capacitive laminates in two- and three-electrode configurations. **(A)** Definition for *I* for a layer bounded between two distances, h_{min} and h_{max}, from neutral plane in a bending laminate. **(B–D)** The concept of *EI* variation upon EHD medium transfer for two- and three-electrode capacitive laminates in left and right column, respectively. **(B)** Uncharged laminates exhibit uniform elastic modulus and, due to mirror symmetry, develop a neutral layer (depicted as a dashed black line) in the centre of the laminate. **(C)** Upon charging, the EHD medium is displaced (blue dashed arrows) between surfaces (two-electrode configuration, left) or between the interior and surface (three-electrode configuration, right). The variation in the swelling ratio is represented by a colour gradient ranging from light cyan to dark cyan, and the membrane is indicated in orange. **(D)** Cross-surface EHD transfer results in negligible EI change in the laminate (two-electrode configuration, left), whereas interior-direction transfer increases the EI of the laminate (three-electrode configuration, right). Up and down arrows indicate the augmentation and diminution of the corresponding property, respectively.

Aldrich) and 40 mL 4-methyl-2-pentanone (MP, 99%, Alfa Aesar) on a magnetic stirrer at 70°C for 24 h.

Electrode suspension was prepared in three steps. First, component A was prepared by dissolving 2 g of PVDF-HFP in 24 mL of MP on a magnetic stirrer at 70°C for 24 h. In parallel, component B was prepared by dispersing 1.75 g of carbon black (BP-2000, ANR Technologies) in 2 g of [EMIM][OTf] and 10 mL of MP at 70°C for 24 h on a magnetic stirrer. Finally, components A and B were mixed.

Spray-deposition of electrode and membrane layers. The preheated (approximately 60°C–65°C) electrode suspension or membrane solution was sprayed using an airbrush (Iwata Revolution HP-TR2) from a distance of about 15 cm for 5 s, keeping the airbrush perpendicular to the surface.

Fabrication of the internal electrode with the current collector. Gold foil on a transfer paper (thickness ~100 nm, Giusto Manetti Battiloro 24K) was cut with scissors into rectangular strips of 4 mm width and taped to a glass substrate, gold side facing up, from one end (Figure 3A). Three layers of electrodes were sprayed on the gold foil (Figure 3B). After each spraying, the glass substrate was placed face down on a paper tissue to prevent out-of-plane deformation and cracking during drying. An infrared lamp was used to accelerate the evaporation of solvents. A membrane layer was formed by spraying six layers of membrane solution (Figure 3C). Next, the outer electrode was formed by spraying three layers of electrode suspension, and the laminate was flipped over (Figure 3D). Then, pieces of transfer paper were used to mask contact. The steps C and D were repeated on the other side. Next, outer current collectors were attached to both sides of the sample using a thin sprayed layer of membrane solution as a glue (Figure 3F). A metal tube (approx. 3 cm diameter) was rolled over the sample to improve current collector adhesion. Then, the laminate was left to dry under the infrared lamp on a paper towel, with a glass plate placed on top as a weight, for a minimum of 12 h (Figure 3G). Finally, the laminate was cut into samples of 4 mm width (Figure 3H). The thickness of the laminate was approximately 420 μm.

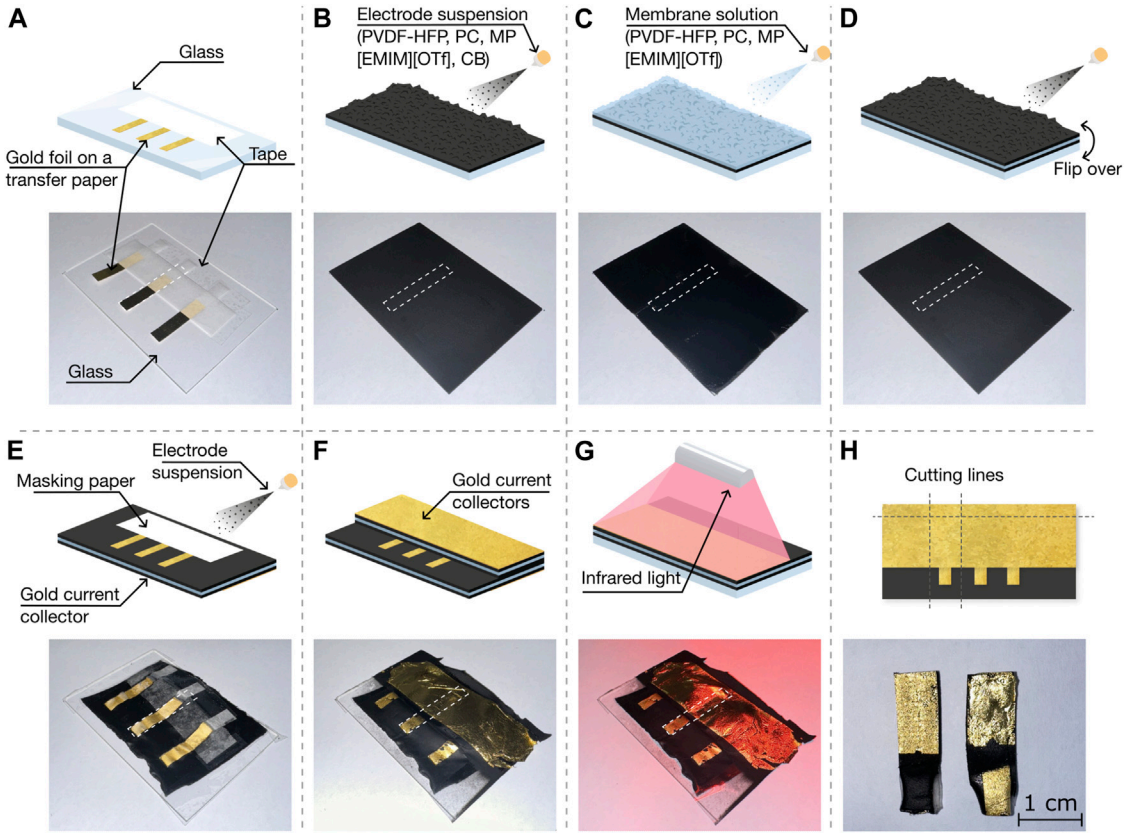

FIGURE 3
Assembly of three-electrode variable-stiffness capacitive laminate and corresponding photographs depicting each step of fabrication. **(A)** Attachment of the gold current collectors to the glass substrate. **(B)** Spray-deposition of electrode suspension on the gold current collector strips. **(C)** Spray-deposition of membrane solution on the previously deposited electrode. **(D)** Spray-deposition of the electrode (external) and flipping over of electrode-membrane-electrode laminate. **(E)** Masking of the contact area for the internal electrode; repetition of steps C-D; spray-deposition of the second external electrode. **(F)** Attachment of outer current collectors to both sides of the laminate. **(G)** Drying under infrared light. **(H)** Definition of samples by cutting. White dashed rectangles indicate the location of a single sample (out of three depicted).

2.2 Input signal

Figure 4 shows the measurement setup. The laminate was mounted between electrically conductive clamps, forming a cantilever. Potentiostat BioLogic BP-300 generated a triangular voltage waveform at a scan rate of 10 mVs^{-1} and a range of ±2 V. The counter-electrode terminal was connected to the inner electrode of the ICL, while the outer electrodes were connected together to the working electrode terminal.

2.3 Bending stiffness measurement

The cantilever was bent sinusoidally (amplitude: 0.36 mm) at a distance l = 9 mm from the base, perpendicular to the surface, at frequency f = 10 Hz using a voice coil actuator (extracted from a commercial CD drive). A laser distance sensor confirmed a negligible effect of the laminate's bending stiffness on voice coil actuation. A custom force sensor constructed of two 350-Ω strain gauges, as detailed in (Must et al., 2019), was attached between the voice coil actuator and the sample. The force amplitude used in bending stiffness measurement was approximately 27 μN and the noise floor of the force sensor was estimated to be 0.68 μN, resulting in a high signal-to-noise ratio of 40. A force offset of approximately 120 μN was applied to ensure continuous contact. The voice coil input signal was generated, and the force sensor data was digitized using a National Instruments USB-6218 data acquisition device and processed in LabVIEW programming environment. The force was sampled at a rate of 10 kHz, resulting in 1,000 force samples per strain cycle and 8,000 sinusoidal strain cycles per voltammetry cycle. The force amplitude (ΔF) was extracted by fast Fourier transformation (FFT) for each ten bending cycles. Bending stiffness EI was calculated according to the Euler-Bernoulli theorem (Goodno and Gere, 2020) as follows:

$$EI = Fl/3\delta_{\max} \quad (1)$$

where F is the load acting on the free end of the cantilever beam at length l from the base, and δ_{max} is the beam's maximum deflection resulting from the load's application, as illustrated in Figure 4.

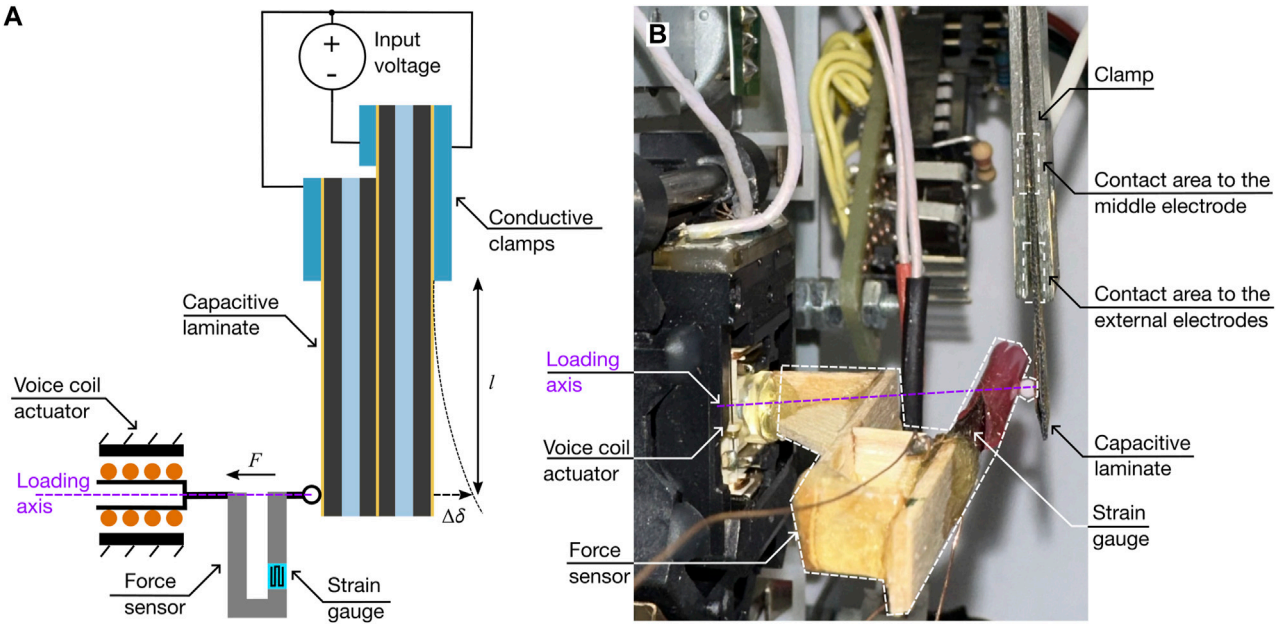

FIGURE 4
Schematic of the measurement setup for bending stiffness variation **(A)** and photograph of the experimental setup **(B)**. A voice coil actuator deforms the free end of the laminate to displacement $\Delta\delta$. The resulting force F is measured with a force sensor attached between the actuator and the laminate.

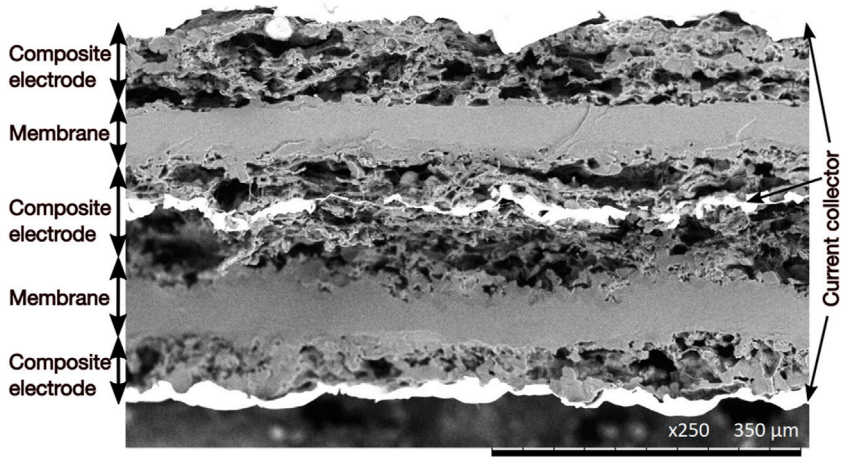

FIGURE 5
Scanning electron microscopy image of the cross-section of capacitive laminate.

2.4 Micrographing

The samples were cryogenically frozen by immersing into liquid nitrogen and then broken while immersed in liquid nitrogen using tweezers. The fracture surface was observed using a tabletop scanning electron microscope (Hitachi TM3000) at 15 keV acceleration voltage.

3 Results

The cross-section of an assembled laminate in Figure 5 confirms the formation of a three-electrode structure. The carbon-free membrane layer (approx. 70 µm) is well-distinguishable from the electrode layers by its smooth structure, almost featureless at the observed magnification. The thickness of the overall laminate and

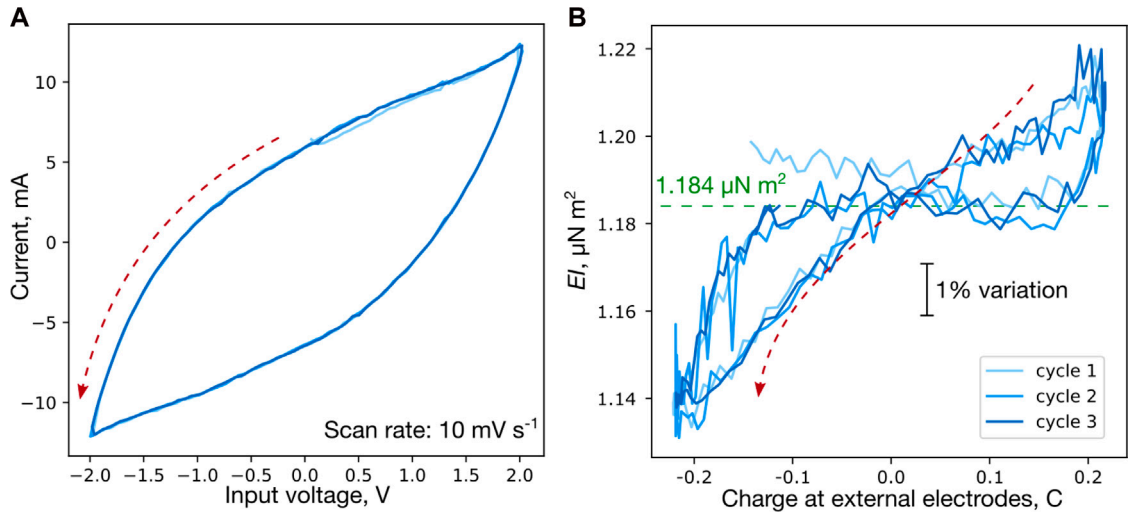

FIGURE 6
Cyclic variation of *EI* of a three-electrode capacitive laminate in response to a triangular input voltage. **(A)** Cyclic voltammetry curve (at 10 mV s^{-1} scan rate). **(B)** Variation of *EI* with respect to applied charge. The Red dashed line indicates the direction of bending stiffness variation **(B)** and the corresponding charge direction in the cyclic voltammetry curve **(A)**, respectively. The purple dashed horizontal line indicates the reference level of the uncharged capacitor.

each individual electrode and membrane layer is homogenous, confirming a successful spray deposition.

The thickness of the middle electrode (approx. 120 μm) is close to the two outer electrodes combined (approx. 135 μm). These thicknesses are optimal for the use case, with the outer electrodes electrically connected (via external wire connection) and polarized with respect to the middle electrode. Consequently, the system can be treated using an electrical equivalent of two capacitors of equal value connected in series. Similar capacitance values provide the highest operating voltage (previous studies confirm mirror-symmetric capacitance-potential profile (Kaasik et al., 2013) of the oppositely polarized electrodes).

The thin gold current collector at the centre of the middle electrode, corresponding to the saturated white region in Figure 5, showed an uneven profile, evidencing conformance to the gold foil to particulate carbon but not *vice versa*. An uneven current collector profile potentially compromises its electrical conductivity; however, as the used gold foil is manufactured by mechanical thinning, it has acquired a locally discontinuous structure that allows for a local stretch without loss of electrical integrity. The current collectors at surfaces show a similar wavy profile as in the middle. Due to the discontinuous metallographic structure, the gold foil only partially blocks the cross-current-collector mobility of liquids. In outward-inward pumping, liquid mobility is not expected across the middle plane of the laminate; thus, the continuity of the middle current collector, regardless of its profile, is not a concern. In the case of two current surface collectors, the microscopic discontinuity of the current collector needs to be considered as a probable mechanism allowing for liquid and gas flow between the environment and the laminate interior. Prevention of fluid pressure buildup is an important optimization parameter.

The electrodes display an extremely rough profile, possibly most influenced by the substantial aggregation of the carbon black particles in sequential steps of spray application. A hierarchical porosity profile, with a broad distribution of pores up to macropores in several tens of μm, is essential for pumping kinetics, as the relatively homogenous membrane is responsible for pressure buildup and maintenance of swelling gradients (by reducing the back flow), whereas the composite electrodes incorporating also larger pores allow relatively fast equilibration of liquid content within each electrode layer. This way, the parts of the carbon-polymer composite far from the membrane acquire a faster swelling profile due to liquid rearrangement due to the inter-electrode capillarity.

The cyclic voltammetry graph (Figure 6A) shows a highly repeatable process, approaching a rectangular shape without revealing any peaks that would indicate the presence of Faradaic processes. However, as the system was exposed to ambient air, moisture content, and thus a small contribution by water splitting is inevitable. Although exposure to ambient humidity complicates the practical application due to a variable viscosity (and thus charge-transfer kinetics, previously extensively researched (Must et al., 2014)), we assign strategic importance to the environment exposure, as leveraged to encapsulation, as free access prevents gas and liquid pressure buildup. Even in the case of a completely non-gassing electrochemical apparatus (Sachan et al., 2014), dynamic swelling anticipates the presence of empty pores to be filled upon liquid influx and, *vice versa*, the void needs to be filled after liquid outflux. Devising specialized flow-return systems can be impractical for highly integrated solutions and would compromise the overall advantage of simple deployment by spraying. Consequently, exposure to the environment is beneficial for performance. Even further, exposed operation

prevents an undesired bending stiffness increase from the encapsulation layers.

After 12 h of exposure to infrared light, the volatile solvent in the electrolytic solution is completely evaporated, and an equilibrium condition of the electrolytic solution composition is achieved. Immediately after electrode or membrane layers deposition, the electrolytic solution is in the most diluted state, and all pores are assumed to be completely filled. When the porous structure is entirely filled with the electrolytic solution, the displacement of the electrolyte is most efficient, but this does not effectively translate into a swelling gradient. Drying the laminate between tissue papers to prevent out-of-plane deformations affects the composition of the electrolytic solution by increasing its saturation with electrolyte and decreasing the pore fill ratio due to evaporation of the volatile solvent (MP). Our hypothesis suggests that evaporation of the volatile solvent improves electrohydrodynamic medium displacement efficiency, leading to enhanced swelling performance through bulk transfer between empty pores, until excessive emptying causes hindered electrolytic solution displacement, increasing electrolytic resistance, resulting in decreased transfer rate and energetic inefficiency.

The bending stiffness measurement was performed at 10 Hz. This frequency is a trade-off between an increased loss tangent at high frequencies due to the viscoelastic nature of the material and the higher signal resolution at the low measurement frequency (Hackl et al., 2005).

A cyclic charging pattern using a triangular input voltage induced an 8-shaped curve in the bending stiffness *EI* variation, which evolves in an anticlockwise direction, as depicted in Figure 6B. The application of a positive charge to outer electrodes (with respect to a single inner electrode) resulted in an increase in bending stiffness (evidencing liquid outflux and deswelling), confirming cation-dominated liquid displacement (liquid influx at positive applied potential) and non-thermal nature (in Joule heating, a symmetric response would be expected). The bending stiffness varied in a range between 1,220 nN mm^2 to 1,131 nN mm^2, corresponding to a deviation of 3.04% to −4.47% from the initial (i.e., uncharged) state. A sharper increase in bending stiffness observed near the maximum applied potential (±2 V) in the dynamic charging experiment is attributed to an increased ionic current, increasing liquid flux. Indeed, the highly dynamic nature of the system implies that diffusive backflow always competes with dynamic ion displacement.

A phenomenologically similar 8-shaped hysteresis curve was previously reported on electrosorption-driven osmotic actuators (Must et al., 2019). In osmotic actuation, concentration gradients result in osmotic potential and pressure; however, in the three-electrode laminate, the contribution of a concentration gradient as the pressure-generation mechanism is not expected to be significant. The open porous structure of the system permits the displacement of the electrolytic solution at a minimal accumulation of pressure. Due to the relatively high ratio between the total amount of ions in the system and the total area of electrode active surface area (carbon black surface area is approximately 1,500 m^2 g^{-1} (Delgado et al., 2016)), the concentration of [EMIM][Otf] in plasticizer is expected to undergo a significant decrease upon charging. During the voltammetry cycle conducted in the experiment, it was observed that the concentration of the electrolytic solution varied by approximately 55%; however, a significant amount of electrolyte was still present in the laminate. Nevertheless, due to a lack of a semipermeable membrane in the system, a substantial osmotic pressure gradient is not expected, and the bending stiffness modulation effect is primarily accounted for the bulk flow of liquid electrolytic medium between different layers. Previous studies on human skin have provided evidence that the electro-osmotic effect can cause bulk directional liquid flow in a porous polymeric matrix with a surface charge, resulting in swelling and elastic modulus gradients that can be detected through an increase in impedance (Grimnes, 1983; Pabst et al., 2019).

Due to its structural and operational symmetry, the three-electrode system did not exhibit bending actuation. However, it showed a significant variation of *EI* (shown in Figure 2C) due to reciprocal variation of elastic modulus and second moment of inertia during electrohydrodynamic medium transfer. The second moment of inertia of external electrodes is higher than the internal due to the larger distance from the neutral plane; therefore, the external electrodes are more susceptible to *EI* variation in the whole laminate beam.

For the design of EHD-based variable stiffness laminates, the following characteristic features are to be taken into consideration. A moderate range of bending stiffness variation is likely the result of the design choice for the highest integration. The high loading (1:1 mass ratio for solid components) of relatively stiff carbon particles (not expected to undergo bending stiffness modulation) in the electrode composite may obscure the effect of swelling of a softer polymeric matrix on overall bending stiffness. Thus, a strategic lateral separation of pumping and stiffness-modulating components may be necessary.

Another distinct feature is the non-optimal combination of the expandable polymeric matrix and the electrohydrodynamic medium. The present selection of a moderately hydrophobic polymer (PVDF-HFP) and the hydrophilic [EMIM][OTf] electrolyte implies no drastic swelling effects consistent with the observed response magnitude. To achieve a more pronounced bending stiffness response, the interaction between the matrix and the electrolytic solution should be sufficiently strong while also being weak enough for reversibility. For faster kinetics, the pore size distribution of the open-porous matrix, and the control over the porosity characteristics during spray-deposition, could be optimized. The search for more suitable combinations is ongoing. This research primarily consolidates the proof-of-principle of electrokinetically driven swelling. Evidence of fast and reversible swelling of biopolymers, such as found in the bacterial cortex (Liu and Chen, 2022) supports the direction of fostering more sustainable and safer robotic materials.

Field-induced transfer of ions accommodates electrolytic solution displacement, and the volume of the polymeric matrix and transferable electrolytic solution determine the largest efficient size of the pumping system. The total amount of electrolytic solution that can be transferred in a pumping system is limited by the surface area of amorphous carbon and the amount of electrolyte, and the largest efficient size of the pumping system is determined by the amount of electrolyte. Once the electrolyte is depleted from the electrolytic solution due to the formation of an electrical double layer, the pumping process is stopped, thus posing a limitation for

continuous mode operation. Consequently, variable stiffness systems based on this approach are primarily suitable for dynamic scenarios of bending stiffness modulation.

4 Discussion

This work presents a pathway to broaden the application scope of porous materials that reversibly swell upon exposure to liquids: the swelling mechanism that previously was considered subject only to external (environment-driven) control is complemented with internal control. Indeed, generating, controlling, and maintaining swelling gradients in an anisotropic open-porosity polymeric matrix (resembling a sponge) is surprising, even more so at a high resolution, and thus has previously received little research attention, although the benefits in the applicable material selection, including biomaterials, are motivating. We suggest a matched internal control mechanism for reversible swelling: electrohydrodynamic rearrangement of liquids. The concept was exemplified on a variable-stiffness three-electrode laminate that can be tuned by charge.

The polarity of the observed stiffness variation–liquid influx caused swelling and thus softening–serves to distinguish the mechanism from pressure-driven (turgor-inspired) variable-stiffness mechanisms that develop a higher stiffness (turgidity) upon liquid influx (based on fluidic pressure acting on a flexible boundary). As both swelling and internal pressurisation result in a positive strain difference, actuators (such as the IPMC) could benefit from both effects, yet deconvolution of these mechanisms is more challenging. However, in consideration of stiffness modulation, swelling and internal pressurization have a counteractive effect, and the prevalent mechanism defines the polarity (and allows for its identification). The swelling mechanism also determines contrary optimization criteria: whereas pressurization-driven variable-stiffness systems demand pressure preservation within closed boundaries, swelling-based variable-stiffness systems benefit from the openness of a porous network for faster kinetics (still with pores small enough to resist spontaneous backflow), even allowing for the working liquid to (temporarily) escape the system, as recalled from Figure 1.

We chose electroosmosis combined with electrosorption for internal liquid rearrangement as the most mechanically and chemically compliant and reversible integrated mechanism. It is worth noting that the mechanically stiff carbon, as one component in the composite electrode, limits the achievable bending stiffness variation. Ideally, the compliance of components responsible for liquid displacement (in this work, carbon electrodes) should be maximised to restrict the bending the least. In the case of the composite electrode approach in this work, the components responsible for pumping and changing stiffness share the same volume, and the elastic modulus of the electrode material exceeds that of the polymer matrix, limiting the available stiffness variation. Moreover, as the pumping performance of the electrosorption-driven pump is proportional to the specific surface area, the carbon loading is maximized, compromising stiffness variation magnitude. In this work, we chose the best compromise between carbon loading (i.e., the high specific surface area, gaining in pumping magnitude) and the resulting increase in composite electrode stiffness.

The modular approach introduced in this work allows also for laterally separating the pumping apparatus from the layers responsible for stiffness variation. The variable swelling ratio of a sole open-porous polymeric membrane disentangled from the pumping system has already been demonstrated in our previous studies, reaching dynamic pore fill ratio variation up to 10% (Sarokin et al., 2023). Yet, the fabrication of a full system with a laterally separated pumping apparatus is more challenging, favoring the composite approach due to being readily available. A capacitive laminate with three electrodes, where the external electrodes are oppositely charged with respect to the internal one, allows for bending stiffness modulation due to asymmetric variation of the second moment of inertia and elastic modulus of external electrodes; in contrast, the potential variation of these properties within the internal electrode has minimum impact on the variation of bending stiffness of three-electrode laminate. The bending stiffness variation upon charge application varied approximately by 7%, confirming the proof of concept and promising improvement by optimization of the composition of the electrolytic solution, the pore size, shape, distribution, and pore filling ratio.

This study provides a new perspective on the development of charge-controlled soft robotic systems, which allow for dynamic variation of mechanical compliance locally, at high resolution in the thickness direction, demonstrating the resolution of approximately half of the laminate thickness (200 μm). This resolution is only approximately one order of magnitude larger than the characteristic size of cells that develop structural rigidity variation by change of turgor (Dumais and Forterre, 2012). The physiological significance of high-resolution swelling gradients in organisms is not universally understood. Yet the possibility of achieving a swelling gradient has been demonstrated in a comparable (skin thickness) scale. The few-hundred-micrometer resolution is still smaller than conveniently achievable with individually defined (possibly using soft lithography) and controlled pressurized chambers, especially in distributed settings. The system is characterized by high reversibility, as no unsolicited redox reactions were observed. Our findings suggest that polymer swelling due to the electrosorption-induced displacement of an electrohydrodynamic medium is a promising mechanism for non-thermal material-level charge-driven bending stiffness control. In the long perspective, the simple construction, reversibility, and non-thermal nature make the charge-controlled material-level stiffness variation attractive for various body-interfaced and wearable applications, e.g., exoskeletons.

Data availability statement

The original contributions presented in the study are included in the article/Supplementary Material, further inquiries can be directed to the corresponding author.

Author contributions

YS and IM developed the original concept. YS designed and constructed the experimental custom apparatus, prepared the three-

electrode laminate, and conducted all experiments. YS and IM interpreted the results and wrote the first version of the manuscript. All authors contributed to the manuscript revision and approved the submitted version.

Funding

This work was supported by the Estonian Research Council grants (PRG1498 and PRG1084) and H2020 project TWINNIMS (Grant agreement 857263).

Conflict of interest

The authors declare that the research was conducted in the absence of any commercial or financial relationships that could be construed as a potential conflict of interest.

The author (AG-N) declared that they were an editorial board member of Frontiers at the time of submission. This had no impact on the peer review process and the final decision

Publisher's note

All claims expressed in this article are solely those of the authors and do not necessarily represent those of their affiliated organizations, or those of the publisher, the editors and the reviewers. Any product that may be evaluated in this article, or claim that may be made by its manufacturer, is not guaranteed or endorsed by the publisher.

Supplementary material

The Supplementary Material for this article can be found online at: https://www.frontiersin.org/articles/10.3389/fmats.2023.1220421/full#supplementary-material

References

Althoefer, K. (2018). Antagonistic actuation and stiffness control in soft inflatable robots. *Nat. Rev. Mater.* 3, 76–77. doi:10.1038/s41578-018-0004-0

Blanc, L., Delchambre, A., and Lambert, P. (2017). Flexible medical devices: review of controllable stiffness solutions. *Actuators* 6, 23. doi:10.3390/act6030023

Delgado, P. A., Brutman, J. P., Masica, K., Molde, J., Wood, B., and Hillmyer, M. A. (2016). High surface area carbon black (BP-2000) as a reinforcing agent for poly [(−)-lactide]. *J. Appl. Polym. Sci.* 133. doi:10.1002/app.43926

Dumais, J., and Forterre, Y. (2012). "Vegetable dynamicks": the role of water in plant movements. *Annu. Rev. Fluid Mech.* 44, 453–478. doi:10.1146/annurev-fluid-120710-101200

Fiorello, I., Del Dottore, E., Tramacere, F., and Mazzolai, B. (2020). Taking inspiration from climbing plants: methodologies and benchmarks—a review. *Bioinspir Biomim.* 15, 031001. doi:10.1088/1748-3190/ab7416

Goodno, B. J., and Gere, J. M. (2020). *Mechanics of materials*. Boston: Cengage learning.

Grimnes, S. (1983). Skin impedance and electro-osmosis in the human epidermis. *Med. Biol. Eng. Comput.* 21, 739–749. doi:10.1007/bf02464037

Hackl, C. M., Tang, H. Y., Lorenz, R. D., Turng, L. S., and Schroder, D. (2005). A multidomain model of planar electro-active polymer actuators. *IEEE Trans. Ind. Appl.* 41, 1142–1148. doi:10.1109/tia.2005.853384

Hao, L., Xiang, C., Giannaccini, M. E., Cheng, H., Zhang, Y., Nefti-Meziani, S., et al. (2018). Design and control of a novel variable stiffness soft arm. *Adv. Robot.* 32, 605–622. doi:10.1080/01691864.2018.1476179

Hao Y, Y., Wang, T., Xie, Z., Sun, W., Liu, Z., Fang, X., et al. (2018). A eutectic-alloy-infused soft actuator with sensing, tunable degrees of freedom, and stiffness properties. *J. Micromech. Microeng.* 28, 024004. doi:10.1088/1361-6439/aa9d0e

Helps, T., Taghavi, M., Wang, S., and Rossiter, J. (2020). Twisted rubber variable-stiffness artificial muscles. *Soft Robot.* 7, 386–395. doi:10.1089/soro.2018.0129

Jiang, A., Ranzani, T., Gerboni, G., Lekstutyte, L., Althoefer, K., Dasgupta, P., et al. (2014). Robotic granular jamming: does the membrane matter? *Soft Robot.* 1, 192–201. doi:10.1089/soro.2014.0002

Kaasik, F., Tamm, T., Hantel, M. M., Perre, E., Aabloo, A., Lust, E., et al. (2013). Anisometric charge dependent swelling of porous carbon in an ionic liquid. *Electrochem. Commun.* 34, 196–199. doi:10.1016/j.elecom.2013.06.011

Kim, P., Kwon, K. W., Park, M. C., Lee, S. H., Kim, S. M., and Suh, K. Y. (2008). Soft lithography for microfluidics: a review. *Biochip J.* 2, 1–11.

Li, Y., Chen, Y., Yang, Y., and Wei, Y. (2017). Passive particle jamming and its stiffening of soft robotic grippers. *IEEE Trans. Robot.* 33, 446–455. doi:10.1109/TRO.2016.2636899

Liu, Z. L., and Chen, X. (2022). Water-content-dependent morphologies and mechanical properties of Bacillus subtilis spores' cortex peptidoglycan. *ACS Biomater. Sci. Eng.* 8, 5094–5100. doi:10.1021/acsbiomaterials.2c01209

Loeve, A. J., Bosma, J. H., Breedveld, P., Dodou, D., and Dankelman, J. (2010). Polymer rigidity control for endoscopic shaft-guide 'Plastolock'—a feasibility study. *J. Med. Device.* 4, 045001. doi:10.1115/1.4002494

Manti, M., Cacucciolo, V., and Cianchetti, M. (2016). Stiffening in soft robotics: a review of the state of the art. *IEEE Robot. Autom. Mag.* 23, 93–106. doi:10.1109/MRA.2016.2582718

Mengaldo, G., Renda, F., Brunton, S. L., Bächer, M., Calisti, M., Duriez, C., et al. (2022). A concise guide to modelling the physics of embodied intelligence in soft robotics. *Nat. Rev. Phys.* 4, 595–610. doi:10.1038/s42254-022-00481-z

Metze, F. K., Sant, S., Meng, Z., Klok, H. A., and Kaur, K. (2023). Swelling-activated, soft mechanochemistry in polymer materials. *Langmuir* 39, 3546–3557. doi:10.1021/acs.langmuir.2c02801

Must, I., Sinibaldi, E., and Mazzolai, B. (2019). A variable-stiffness tendril-like soft robot based on reversible osmotic actuation. *Nat. Commun.* 10, 344. doi:10.1038/s41467-018-08173-y

Must, I., Vunder, V., Kaasik, F., Põldsalu, I., Johanson, U., Punning, A., et al. (2014). Ionic liquid-based actuators working in air: the effect of ambient humidity. *Sens. Actuators B Chem.* 202, 114–122. doi:10.1016/j.snb.2014.05.074

Pabst, O., Martinsen, Ø. G., and Chua, L. (2019). Information can be stored in the human skin memristor which has non-volatile memory. *Sci. Rep.* 9, 19260. doi:10.1038/s41598-019-55749-9

Punning, A., Vunder, V., Must, I., Johanson, U., Anbarjafari, G., and Aabloo, A. (2016). *In situ* scanning electron microscopy study of strains of ionic electroactive polymer actuators. *J. Intell. Mater. Syst. Struct.* 27, 1061–1074. doi:10.1177/1045389x15581520

Qin, D., Xia, Y., and Whitesides, G. M. (2010). Soft lithography for micro-and nanoscale patterning. *Nat. Protoc.* 5, 491–502. doi:10.1038/nprot.2009.234

Sachan, V. K., Singh, A. K., Jahan, K., Kumbar, S. G., Nagarale, R. K., and Bhattacharya, P. K. (2014). Development of redox-conducting polymer electrodes for non-gassing electro-osmotic pumps: a novel approach. *J. Electrochem. Soc.* 161, H3029–H3034. doi:10.1149/2.0071413jes

Sarokin, Y., Aabloo, A., and Must, I. (2023). Plant-inspired rearrangement of liquid in a porous structure for controlled swelling. *Bioinspir. Biomim.* 18, 066005. doi:10.1088/1748-3190/acf633

Saunier, J., Alloin, F., Sanchez, J. Y., and Barriere, B. (2004). Plasticized microporous poly (vinylidene fluoride) separators for lithium-ion batteries. I. Swelling behavior of dense membranes with respect to a liquid electrolyte—characterization of the swelling equilibrium. *J. Polym. Sci. B Polym. Phys.* 42, 532–543. doi:10.1002/polb.10730

Shimizu, H., Arioka, Y., Ogawa, M., Wada, R., and Okabe, M. (2011). Sol-gel transitions of poly (vinylidene fluoride) in organic solvents containing LiBF4. *Polym. J.* 43, 540–544. doi:10.1038/pj.2011.21

Shiva, A., Stilli, A., Noh, Y., Faragasso, A., De Falco, I., Gerboni, G., et al. (2016). Tendon-based stiffening for a pneumatically actuated soft manipulator. *IEEE Robot. Autom. Lett.* 1, 632–637. doi:10.1109/LRA.2016.2523120

Uduste, I., Kaasik, F., Johanson, U., Aabloo, A., and Must, I. (2020). An all-textile non-muscular biomimetic actuator based on electrohydrodynamic swelling. *Front. Bioeng. Biotechnol.* 8, 408. doi:10.3389/fbioe.2020.00408

Wang, L., Yang, Y., Chen, Y., Majidi, C., Iida, F., Askounis, E., et al. (2018). Controllable and reversible tuning of material rigidity for robot applications. *Mater. Today.* 21, 563–576. doi:10.1016/j.mattod.2017.10.010

Wang, T., Zhang, J., Li, Y., Hong, J., and Wang, M. Y. (2019). Electrostatic layer jamming variable stiffness for soft robotics. *IEEE/ASME Trans. Mechatron.* 24, 424–433. doi:10.1109/TMECH.2019.2893480